HHS Public Access

Author manuscript

Clin Cancer Res. Author manuscript; available in PMC 2018 March 05.

Published in final edited form as:

Clin Cancer Res. 2017 July 15; 23(14): 3781–3793. doi:10.1158/1078-0432.CCR-16-1716.

Preclinical development of a non-toxic oral formulation of monoethanolamine, a lipid precursor, for prostate cancer treatment

Roopali Saxena[1], **Chunhua Yang**[1], **Mukkavilli Rao**[1], **Ravi Chakra Turaga**[1], **Chakravarthy Garlapati**[1], **Sushma Reddy Gundala**[1], **Kimberly Myers**[1], **Ahmed Ghareeb**[1], **Shristi Bhattarai**[1], **Golnaz Kamilinia**[1], **Sangina Bristi**[1], **Dan Su**[2], **Giovanni Gadda**[2], **Padmashree C. G. Rida**[1], **Guilherme H. Cantuaria**[3], and **Ritu Aneja**[1,*]

[1]Department of Biology, Georgia State University, Atlanta, GA-30303

[2]Department of Chemistry, Georgia State University, Atlanta, GA-30303

[3]Department of Gynecologic Oncology, Northside Hospital Cancer Institute, Atlanta, GA-30342

Abstract

Purpose—Most currently-available chemotherapeutic agents target rampant cell division in cancer cells, thereby affecting rapidly-dividing normal cells resulting in toxic side-effects. This non-specificity necessitates identification of novel cellular pathways that are reprogrammed selectively in cancer cells and can be exploited to develop pharmacologically superior and less-toxic therapeutics. Despite growing awareness on dysregulation of lipid metabolism in cancer cells, targeting lipid biosynthesis is still largely uncharted territory. Herein, we report development of a novel non-toxic orally-deliverable anticancer formulation of monoethanolamine (Etn), for prostate cancer by targeting the Kennedy pathway of phosphatidylethanolamine (PE) lipid biosynthesis.

Experimental Design—We first evaluated GI-tract stability, drug-drug interaction liability, pharmacokinetic and toxicokinetic properties of Etn to evaluate its suitability as a non-toxic orally-deliverable agent. We next performed *in vitro* and *in vivo* experiments to investigate efficacy and mechanism of action.

Results—Our data demonstrate that Etn exhibits excellent bioavailability, GI-tract stability, and no drug-drug interaction liability. Remarkably, orally-fed Etn inhibited tumor growth in four weeks by ~67% in mice bearing human prostate cancer PC-3 xenografts without any apparent toxicity. Mechanistically, Etn exploits selective overexpression of choline kinase in cancer cells, resulting in accumulation of phosphoethanolamine (PhosE), accompanied by downregulation of HIF-1α that induces metabolic stress culminating into cell death.

[*]**Correspondence be addressed to:** Ritu Aneja, Department of Biology, Georgia State University, Atlanta, GA-30303, raneja@gsu.edu; Phone: 404-413-5417; Fax: 404-413-5301.

Conflict of interest statement

The authors declare that there are no conflicts of interests.

Conclusions—Our study provides first evidence for the superior anticancer activity of Etn, a simple lipid precursor formulation, whose non-toxicity conforms to FDA-approved standards, compelling its clinical development for prostate cancer management.

Keywords

Glucose metabolism; Kennedy pathway; monoethanolamine; phosphoethanolamine; prostate cancer

Introduction

Malignant transformation alters several physiological processes including reprogramming of biochemical and metabolic pathways, which can be exploited to develop superiorly efficacious and less-toxic cancer therapies (1, 2). Altered lipid metabolism is one of the hallmarks of cancer. Thus, cellular lipids and lipid biosynthesis enzymes may serve as promising anticancer targets (3, 4). Literature reports that lipids and their precursor-based formulations are attractive anticancer drug candidates. For example, alkylphospholipids (ALPs) exert cytotoxic effects by targeting cell membranes instead of conventional targets like DNA or microtubules (5). Lipid precursors such as omega-3 polyunsaturated fatty acids (ω-3 PUFA) exhibit antiproliferative activity against multiple cancers (6).

Another lipid precursor, phosphoethanolamine (PhosE), has recently garnered a great deal of attention in Brazil (7, 8) and is a subject of intense anticancer research (9–15). PhosE, a biosynthetic precursor of phosphatidylethanolamine (PE) lipids, constitutes the second-most abundant lipid class in cells (16) and is synthesized in the first step of Kennedy pathway of PE lipid biosynthesis through ATP-dependent phosphorylation of monoethanolamine (Etn) (17). PhosE exhibits antitumor activity in various *in vitro* and *in vivo* models by affecting multiple signaling pathways (9–15). Interestingly, vitamin K2-induced apoptosis in Jurkat cells is ascribed to intracellular PhosE accumulation (18).

Herein, we evaluated Etn and PhosE, biosynthetic precursors of PE lipids, as anticancer agents to ultimately develop a non-toxic orally-deliverable formulation for prostate cancer. We found that Etn, first precursor in Kennedy pathway, exhibits remarkable anti-prostate activity in *in vitro* and *in vivo* models. The Lipinski's rule for molecular properties endorsed Etn's appropriateness for oral administration in humans. Mechanistically, Etn induces cell death by downregulation of HIF1-α, accompanied by depletion of cellular glucose and glutamine levels; this results in metabolic stress and triggers apoptosis. Etn spares normal cells by exploiting the cancer cell-specific overexpression of choline kinase, an enzyme that converts Etn to cytotoxic PhosE.

Materials and Methods

Information on Cell Lines

PC-3, DU145, MDA-MB-468, OVCAR-3, CFPAC-1, and HCT116 cancer cell lines were purchased from ATCC and used as such as authentication of the cell lines was provided with their purchase from ATCC.

The LNCaP cell line is the parental cell line and the C4-2 and C4-2B are all derivatives of the LNCaP parental cell line. These cell lines were developed by Leland Chung's group (Cedars-Sinai Medical Center, LA, CA) and were obtained from his lab as a generous gift. C4-2B cells were tested for mycoplasma contamination using MycoAler Mycoplasma Detection Kit from Lonza.

PC-3-luc cells were purchased from Perkin Elmer and periodically tested for mycoplasma contamination using MycoAler Mycoplasma Detection Kit from Lonza.

All experiments were performed with cells between 10–15 passages.

Cell lines, media, antibody and reagents

Prostate (PC-3, PC-3-luc, DU145, C42B), breast (MDA-MB-468), ovarian (OVCAR-3), pancreatic (CFPAC), colon (HCT116) cancer cell lines and near-normal prostate RWPE-1 cells were used. PC-3-luc cells were from Perkin Elmer (Waltham, MA) and all other cell lines were from ATCC. Primary antibodies against Cdk4, Cdk2, p-Rb, p21, Bim, Bid, Bcl-2, pBcl-2, cleaved poly(ADP-ribose)polymerase (PARP) and β-actin were from Cell Signaling (Beverly, MA), Ki67, HIF1-α and p53 were from BD Bioscience (San Jose, CA) and Choline kinase was from Proteintech (Rosemont, IL). Bax, GAPDH and HRP-conjugated secondary antibodies were from Santa Cruz (Santa Cruz, CA). Phosphoethanolamine, monoethanolamine, luciferin and Dimethyloxalylglycine, N-(Methoxyoxoacetyl)-glycine methyl ester (DMOG) were from Sigma (St Louis, MO). Choline kinase-α inhibitor was from Calbiochem (San Diego, CA). siRNA against choline kinase was from GE Dharmacon (Lafayette, CO).

Stability of Etn and PhosE in simulated gastric (SGF) and intestinal fluid (SIF)

SGF and SIF were prepared following US Pharmacopeia methods. PhosE and Etn were incubated in SGF and SIF for varying times followed by their quantification using LC-MS/MS analysis.

Pharmacokinetic (PK) and toxicological studies

PK studies (oral and intravenous) were performed in male BALB/c mice (Harlan, Indianapolis, IN). Plasma was extracted from blood samples collected from animals at different time points by centrifugation (8000g/10 min) and stored below −80°C until analysis. PK parameters were calculated using non-compartmental analysis tool of Phoenix WinNolin® software (V6.3, Pharsight, St Louis, MO). Toxicity studies of Etn were performed in male and female Sprague-Dawley (SD) rats (Harlan, Indianapolis, IN).

Cell proliferation and colony survival assay

Proliferation of PC-3, DU145, C42B, RWPE-1, MDA-MB-468, OVCAR-3 and CFPAC cells treated with Etn/PhosE was evaluated employing MTT assay as described earlier (19). Clonogenic assay was performed as described previously (19).

In vivo tumor growth and bioluminescent imaging

In vivo prostate tumor growth in athymic male BALB/c mice was measured using vernier calipers and bioluminescence imaging as described previously (19). Animal experiments were in compliance with GSU IACUC guidelines.

Immunoblotting and immunohistochemistry

Immunoblotting was performed as described earlier (20). 5 μm prostate tumor sections were stained for Ki67 and c-PARP and prostate cancer TMA (US Biomax, Derwood, MD) was immunostained for choline kinase. All stained slides were examined by a pathologist in a blinded-manner.

In silico analysis of choline kinase expression

Expression level of choline kinase A in prostate cancer was analyzed using Oncomine (https://www.oncomine.org/resource/login.html). Reporter ID and platform for datasets used were as follows: Gene rank 229 (21), 839 (22), 2059 (23), 1589 (24), 8514 (25), 1206 (26), 546 (27) analyzed on Human Genome U133 Plus 2.0 Array.

RNA, cDNA preparation and Real Time-PCR

RNA extracted from control and 2 mg/ml Etn-treated PC-3 cells using RNeasy kit from Qiagen (Hilden, Germany), and quantified using NanoDrop. Reverse transcription of RNA was performed for the first strand cDNA synthesis using first strand synthesis kit (GoScript™ Reverse Transcription System-A5000) from Promega (Madison, WI). The quality of cDNA was checked on agarose gel.

RT-PCR of cDNA samples (in duplicates) was performed using iQ™ SYBR® Green Supermix from Bio-Rad (Hercules, CA) as per manufacturer's instructions. The RT-PCR primers were designed manually, checked with the primer3 software and ordered from Sigma (St Louis, MO).

Measurement of oxygen consumption rate (OCR)

OCR was measured using a computer-interfaced oxygen electrode (Hansatech Instruments Inc., Norfolk, UK) by monitoring initial rate of oxygen consumption at 37°C and atmospheric oxygen concentration (230 μM O_2).

Electron microscopy and lipidomics

Tumor tissue was processed for electron microscopy as described previously (19). Lipidomic analysis of control and Etn-treated tumors was performed by Lipidomics Core Facility, Wayne State University.

Statistical analysis

Results are expressed as mean values ± SE values of at least three independent experiments. p values (Student's *t* test) were calculated using Microsoft Excel software.

Results

PE lipid precursors as anticancer candidates: GI-tract stability, drug-drug interactions and pharmacokinetics

Given that development of oral drugs is impeded by limited solubility, poor GI-tract stability, low permeability and extensive first-pass metabolism (28), we first asked if PE lipid precursors are good candidates for oral delivery. Interestingly, Etn and PhosE both satisfy Lipinski's and Veber's rule that examine molecular properties and druggability of a compound, suggesting that these PE lipid precursors (Supplementary Fig. 1) can induce pharmacological effects in humans upon oral consumption, thus qualifying them as viable candidates for further evaluation.

Many drugs are degraded in the GI-tract when confronted with extreme pH and harsh digestive enzymes, thereby explaining their decreased bioavailability or inability to reach the target at optimal concentrations. Simulated gastric (SGF; pH 1.2) and intestinal (SIF; pH 6.8) fluid mimic GI-tract environment and are amenable *in vitro* systems to evaluate compound degradation in GI-tract (US Pharmacopoeia). We found that both Etn and PhosE were stable in SGF over 1h (Fig. 1Ai). While Etn remained unchanged in SIF over time (Fig. 1Aii), PhosE exhibited a ~35% decrease in its concentration after 2h in SIF suggesting its degradation (Fig. 1Aii). These results demonstrate enhanced stability of Etn compared to PhosE in the GI-tract.

Polypharmacy increases the risk of drug-drug interaction (DDI) and has led to drug marketing with black box warnings (29). Thus, we evaluated the potential of Etn and PhosE to inhibit major drug metabolizing cytochrome P450 enzymes. For all the nine tested CYPs (CYP1A2, CYP2A6, CYP2B6, CYP2C8, CYP2C9, CYP2C19, CYP2D6, CYP2E1 and CYP3A4) Etn and PhosE showed IC_{50} values of more than 100 μM (equivalent to 6.1 μg/ml Etn and 14.1 μg/ml PhosE) suggesting no CYP related drug-drug interaction liabilities (Supplementary Table 1).

Next, we developed a bioanalytical method to quantify Etn and PhosE using LC-MS/MS [representative chromatograms for Etn (Retention Time (RT): 6.3 min) and PhosE (RT: 5.3 min) in Supplementary Fig. 2A]. To select a suitable matrix for pharmacokinetic (PK) studies and to rule out any red blood cell (RBC) accumulation of Etn and PhosE, blood to plasma concentration ratio (BPR) was determined in BALB/c mice. Our data confirmed lack of preferential partitioning into RBCs; hence plasma was selected as matrix for PK studies (Supplementary Fig. 2B).

To evaluate bioavailability, we performed PK studies in BALB/c mice following oral (Etn: 40 mg/kg; PhosE: 60 mg/kg) and intravenous (Etn: 2 mg/kg; PhosE: 3 mg/kg) dose (Supplementary Fig. 2). Irrespective of the compound dosed, we analyzed both Etn and PhosE in all samples. The time to reach peak plasma concentration was 10 min for both Etn and PhosE upon oral Etn administration. Maximum concentration (C_{max}) achieved following oral administration of 40 mg/kg Etn was 32-fold higher at 17.37 ug/ml compared to 0.55 ug/ml of PhosE. Similarly, AUC_{last} of Etn was 13-fold higher at 9.10 ug/ml compared to 0.72 ug/mL of PhosE (Figs. 1Bi,1Bii; Supplementary Table 2). However, oral administration

of PhosE gave similar exposure (C_{max} and AUC_{last}) for both PhosE (1.14 μg/mL and 1.89 μg.h/ml) and Etn (4.32 μg/mL and 2.02 μg.h/ml) suggesting that PhosE gets converted into Etn *in vivo* (Figs. 1Bi,1Bii). A similar trend was observed following intravenous administration of PhosE (Supplementary Table 2). Intravenous Etn led to a moderate clearance at 57.23 ml/min/kg compared to normal liver blood flow of 90 ml/min/kg (Fig. 1Ci). The volume of distribution (V_d) of Etn was 4-fold higher compared to normal body water of 0.7 L/kg confirming its extensive distribution into various tissues (Fig. 1Cii). PhosE showed high clearance of 101.92 ml/min/kg equivalent to normal liver blood flow with a high V_d at 4.82 L/kg (Figs. 1Ci,1Cii). Both Etn and PhosE showed a plasma half-life of less than 1h. While oral bioavailability of Etn was excellent at 78%, PhosE was poorly-bioavailable at 19% (Supplementary Table 2), perhaps due to its conversion to Etn by alkaline phosphatases present in intestine and liver. Summarizing, our PK data strongly suggest Etn's superiority over PhosE for an orally-deliverable agent.

To evaluate concentration-time profile of Etn and to understand its accumulation following repeated oral dosing for 28 days, we used Phoenix WinNonlin software with single dose administration data. Etn showed T_{max} of less than 30 min following daily repeated dose confirming rapid absorption (Supplementary Table 3). No Etn accumulation was predicted on dosing over 28 days. Interestingly, a dose proportional increase in exposure was observed from 40 mg/kg to 200 mg/kg. A two-fold increase in dose (40 mg/kg to 80 mg/kg) elicited a two-fold increase in exposure. Similarly, a five-fold increase (from 40 mg/kg to 200 mg/kg) led to a five-fold increase in exposure on day 1 and day 28. The simulated data profile suggests BID (twice-a-day) dosing regimen for toxicological studies.

We next asked whether Etn is non-toxic, well-tolerated and safe for oral consumption. As per OECD guidelines, we first tested acute toxicity of Etn in male and female Sprague-Dawley (SD) rats. Five male and five female rats were orally administered with single dose of 5 g/kg Etn and monitored for one week for any sign of distress/sickness. After one week, all rats were alive and did not display any sign of distress or toxicity suggesting that Etn does not induce any acute toxicity even at the limit dose. We further investigated organ-related toxicity by histopathological evaluation of organs obtained from control and Etn-fed animals. Comparative analysis of various blood components and serum chemistry parameters indicative of liver, kidney and cardiac function and muscle integrity in control and Etn-fed groups was performed. Immunotoxicity of Etn was evaluated by estimating percentages of CD4-T, CD8-T, CD19-B, NK cells and macrophages in spleens from control and Etn-fed mice. Our data show that Etn feeding did not induce any observable organ-related or immune toxicity and was safe for oral consumption over an extended period (Supplementary Figs. 3–5).

Anti-proliferative activity of PE lipid precursors

Next, we evaluated the antiproliferative activity of various Etn and PhosE concentrations on human prostate PC-3 cancer cells. Quantitation of cell survival showed that Etn was more effective in inhibiting cell proliferation compared to PhosE as shown in Fig. 2Ai. The half-maximal concentration (IC_{50}) of Etn was ~0.88 mg/ml. Interestingly, PhosE only showed limited inhibition of PC-3 cell proliferation up to 0.5 mg/ml; concentrations greater than 0.5

mg/ml were mostly ineffective (Fig. 2Ai). In a clonogenic assay to assess the reproductive capacity of cells upon drug removal, we found that while 2 mg/ml Etn decreased colony numbers by ~97%, 2 mg/ml PhosE was ineffective in decreasing colony numbers compared to control cells (Fig. 2Aii). We further tested antiproliferative activity of Etn on other prostate cancer lines (DU145 and C42B) and near-normal prostate cell line, RWPE-1. We found that 0.5 and 1 mg/ml Etn were more effective in reducing viability of prostate cancer lines (PC-3, DU145 and C42B) compared to normal prostate cells (RWPE-1) (Fig. 2Bi). While 0.5 mg/ml Etn reduced survival of PC-3, DU145 and C42B cells by ~30–52%, RWPE-1 cells remained unaffected. To test the generality of Etn's anti-proliferative activity on representative cancer cell lines from different tissues [breast (MDA-MB–468), ovary (OVCAR-3), and pancreas (CFPAC)], we performed MTT assay to obtain dose-response curves upon Etn treatment. The IC_{50} of Etn was 0.55, 0.29, and 1.9 mg/ml in MDA-MB-468, OVCAR-3 and CFPAC, respectively (Fig. 2Bii) suggesting its broad applicability in inhibiting proliferation of various cancer cell types. Further, PhosE was ineffective in inhibiting proliferation and colony formation of cancer cells of varying tissue-origin (Supplementary Fig. 6). To understand why Etn was more effective than PhosE in inhibiting proliferation, we quantified changes in intracellular levels of PhosE and Etn upon treatment with Etn or PhosE in PC-3 cells. Given that Etn and PhosE are interconvertible, we were curious to pinpoint the species responsible for inhibiting proliferation. Intriguingly, both Etn and PhosE remarkably increased PhosE intracellularly in Etn-treated cells (Fig. 2Ci). While Etn elevated PhosE levels by ~40-fold compared to control cells, PhosE increased intracellular PhosE levels by only ~15-fold relative to control cells (Fig. 2Cii). Thus, higher intracellular PhosE levels clearly correlated with reduced cell survival. These data confirmed that Etn serves as an easily absorbable pro-drug, which upon entry into cells, gets converted into cytotoxic intracellular PhosE.

In vivo efficacy of Etn in prostate cancer xenografts

Given its superior absorption, GI-tract stability, non-toxicity and antiproliferative activity, Etn is clearly a better candidate than PhosE for development of an oral anticancer formulation. However, since PhosE gets converted into Etn upon oral administration, we reasoned that formulations containing both Etn and PhosE may provide a two-fold advantage and could be potentially developed for cancer treatment. Firstly, PhosE converts into Etn *in vivo*, thereby increasing Etn exposure more than Etn alone. Secondly, the acidic nature of PhosE can attenuate the basicity of Etn making it suitable for oral administration. To this end, we tested the *in vivo* efficacy of a repertoire of formulations containing Etn and PhosE in various molar ratios with pH adjusted to 5 or 7.4 using phosphoric acid. Unfortunately, formulations with pH 7.4 and/or containing PhosE were either not as effective in inhibiting tumor growth as Etn at pH 5 or in some cases even accelerated tumor growth (data not shown). Moreover, Etn absorption was independent of pH (5/7.4) or acid (H_3PO_4/HCl/H_2SO_4) employed to adjust formulation pH (Supplementary Table 4). These data generated compelling grounds to exclusively pursue the Etn-containing formulation at pH 5 adjusted using phosphoric acid.

We next examined the *in vivo* anticancer efficacy of Etn formulation in prostate (PC-3-luc and DU145) and colon (HCT116) cancer xenografts. Tumor-bearing control and treated

mice received vehicle (water) and 40 mg/kg Etn, respectively, by oral gavage for 2 (HCT116) or 4 (PC-3-luc and DU145) weeks. Tumor growth was measured by both vernier calipers (twice/week) and bioluminescence imaging (only PC-3-luc; Figs. 3Ai,3Aii) (once/week) for 2/4 weeks. We observed ~67% reduction in tumor volume (Fig. 3Aiii) and ~55% reduction in tumor weight (Fig. 3Aiv) after 4 weeks of Etn treatment in PC-3-luc xenograft model. In DU145 xenografts, we observed a ~42% reduction in tumor volume (Fig. 3Di) and ~29% reduction in tumor weight (Fig. 3Dii) after 4 weeks of Etn treatment. Further, we observed ~44% decrease in tumor volume in HCT116 xenograft model after 2 weeks of Etn treatment (Supplementary Fig. 7A). Importantly, no apparent change in body weight of control and Etn-treated mice over the treatment course in both models (Figs. 3B,3E; Supplementary Fig. 7B) implied that Etn is non-toxic. Quantification of intratumoral levels of Etn and PhosE after 4 weeks of Etn treatment showed that PhosE level in Etn-treated PC-3-luc tumor-bearing mice was ~38% higher than control mice (Fig. 3C). However, we did not observe any significant change in intratumoral Etn levels between control and Etn-treated mice. These data are in consonance with our *in vitro* findings and reconfirm that the intracellular conversion of Etn into PhosE results in intratumoral accumulation of cytotoxic PhosE, which perhaps is crucial for tumor growth inhibition.

Inhibition of choline kinase (CK) activity attenuates Etn's antiproliferative activity

Having confirmed that Etn converts into PhosE intracellularly, we next sought to identify the enzyme responsible for this conversion. Two enzymes, namely, ethanolamine kinase and choline kinase (CK) are known to catalyze conversion of Etn into PhosE. However, CK has been reported to be overexpressed in multiple cancers including lung, prostate and breast (30). To examine if CK catalyzes the conversion of Etn into PhosE, we determined survival of PC-3 cells upon Etn treatment in the presence/absence of CK function. While Etn alone reduced cell proliferation by ~33% (Fig. 4A), pharmacological CK inhibition significantly attenuated Etn-induced reduction in cell proliferation from ~33% to ~17% (Fig. 4A). CK inhibitor itself did not significantly affect PC-3 proliferation at the employed concentration. We also observed that CK inhibition reduced conversion of Etn into PhosE by ~19% (Fig. 4B). We further employed siRNA approach to confirm the role of CK in Etn-induced cell death. Knockdown (KD) of CK using siRNA significantly abated Etn-mediated reduction in viability of PC-3 cells (Fig. 4C). While 0.5 mg/ml Etn reduced cell survival of PC-3 cells by ~38%, cell viability in CK KD PC-3 cells was decreased by only ~11% (Fig. 4C). These results underscore CK's role in the conversion of Etn to PhosE in PC-3 cells. Further, we found that CK expression is low in normal prostate cell line (RWPE-1) compared to prostate cancer cell lines (PC-3, DU145 and C42B) (Fig. 4D), which may underlie differential sensitivity of normal versus cancer cells to Etn (Fig. 2Bi). Next, we asked why Etn selectively affected cancer cells and spared normal ones. To this end, we explored publicly-available datasets for CK gene expression in prostate cancer patients as well as evaluated CK protein expression immunohistochemically in tumor versus adjacent normal tissue from prostate cancer patients. We found that CK is highly overexpressed in prostate cancer tissue compared to adjacent normal (Figs. 4E,4Fi,4Fii). Our in-silico analysis showed that prostate cancer exhibits 2.1-fold higher CK expression compared to normal prostate tissue (Fig. 4E). Quantification of CK immunostaining showed that CK expression was 1.5-fold higher in prostate cancer tissue compared to adjacent normal (Fig. 4Fii). This differential CK

expression (both at gene and protein level) perhaps explains increased sensitivity of cancer cells to Etn.

Etn activates mitochondrially-mediated death pathways and affects cellular respiration and metabolism

To gain mechanistic insights, we evaluated protein expression and transcript levels of cell-cycle and apoptosis regulatory molecules in PC-3 cells using immunoblotting (Figs. 5A, 5B). While Etn caused downregulation of protein expression of pRb, Cdk4, and Cdk2, upregulation of p21 suggested that Etn stalls cell-cycle progression. Further, an increase in protein expression of proapoptotic markers (c-PARP and Bim), and a decrease in antiapoptotic molecules (Bcl-2) upon Etn treatment implicates a mitochondrially-mediated death pathway (Fig. 5A). This was confirmed at transcriptional level where Etn upregulated p21, PARP1, Bax and Bid, and downregulated Bcl-2 (Fig. 5B). The binding of Annexin-V to phosphatidylserine (PS) lipids followed by flipping to the outer plasma membrane leaflet in apoptotic cells (31) serves as an indicator of apoptosis. We observed flow-cytometrically that Annexin-V positive cells increased from ~8% to ~25% upon Etn treatment, suggesting that Etn induces apoptosis in PC-3 cells (Supplementary Fig. 6C). To uncover signaling pathways responsible for *in vivo* tumor inhibition, we examined expression levels of molecular regulators of cell-cycle and apoptosis in tumor lysates prepared from control and 40 mg/kg Etn-treated mice. Etn caused downregulation of p21, Bax and pBcl2 and upregulation of c-PARP, Bim and Bid (Fig. 5C). Since p21, Bax and pBcl2 are downstream effectors of p53, we examined p53 levels in control and Etn-treated tumors as well as p53 transcript levels in control and Etn-treated PC-3 cells. Etn-treated tumors displayed higher expression of p53 compared to control tumors (Fig. 5C). Further, Etn-treated PC-3 cells exhibited 1.2-fold increase in p53 transcript levels compared to controls (Fig. 5B). Upregulation of p53 suggested activation of p53-induced cell growth arrest and apoptosis. Immunohistochemical staining of paraffin-embedded samples for Ki67 (cell proliferation) and c-PARP (apoptotic) showed decrease in Ki67 and increase in c-PARP in treated tumors compared to control ones (Figs. 5Di,5Dii). While ~62% cells were Ki67-positive in control tumors, Ki67 positivity was reduced to ~40% in Etn-treated tumors (Fig. 5Dii).

To address how p53 is activated upon Etn treatment, we extrapolated the *in vitro* efficacy dose (IC_{50}: 0.88 mg/ml) to the corresponding *in vivo* dose (140.57 mg/kg; therapeutic index=5) using NIH guidelines (32). Intriguingly, we realized that supraphysiological Etn concentrations are required for *in vitro* activity. However, Etn displays remarkable *in vivo* efficacy with 40 mg/kg Etn which is ~3.5 times lower than the extrapolated dose for its *in vivo* efficacy. This indicated that Etn takes advantage of an unknown aspect of the *in vivo* physiology of cancer to evoke its anticancer activity, which cannot be mimicked in a cell culture system.

It is well-recognized that HIF1-α plays a pivotal role in cancer progression by regulating several survival pathways in cancer cells (33, 34). For instance, HIF1-α regulates glucose metabolism under hypoxia by inducing expression of glucose transporters to increase glucose uptake to fulfill energy demands of rapidly proliferating cancer cells through glycolysis (35). Recently, HIF1-α has been shown to regulate glutamine metabolism (36).

Reports indicate that p53 pathway is activated upon energetic/metabolic stress in cells (37). Literature also indicates that cellular PhosE accumulation affects respiration and that both Etn and PhosE impair mitochondrial respiration by altering oxygen consumption rate (OCR) in isolated mitochondria (38, 39). This led us to hypothesize that PhosE accumulation alters HIF1-α function that impairs glucose/glutamine metabolism leading to bioenergetic/metabolic stress in cells, which activates p53-induced cell death. To test this hypothesis, we examined HIF1-α protein and gene expression in Etn-treated tumors and PC-3 cells, respectively. We found that Etn treatment resulted in 50-fold reduction in HIF1-α transcripts levels in PC-3 cells compared to control cells (Fig 5B). We found downregulation of HIF1-α protein expression in Etn-treated tumors compared to control tumors (Fig. 5E). Using DMOG, we tested the effect of HIF1-α stabilization (active HIF1-α signaling) on Etn-mediated cell death in PC-3 cells. Etn was more effective in reducing survival in PC-3 cells with active HIF1-α signaling owing to HIF1-α stabilization by DMOG compared to controls (Fig. 5F), suggesting the possible role of HIF1-α signaling axis in Etn-mediated cell death. These data lend plausible explanation for the discrepancy between *in vitro* and *in vivo* efficacy doses. It is likely that Etn is more effective *in vivo* due to active HIF1-α signaling in hypoxic tumor tissues compared to cultured cells under normoxic condition. Further, we measured OCR in control and Etn-treated cells as a function of cell number as well as evaluated glucose and glutamine content in cultured cells and tumors from control and Etn-treated mice. We observed that Etn affected OCR in PC-3 cells and the extent of reduction varied with cell number such that OCR in treated cells was reduced by ~26% compared to controls at a concentration of 1 million cells/ml (Fig. 5G). Both glucose and glutamine content were also significantly reduced in Etn-treated tumors (Figs. 5Hi,5Hii) and cells (Figs. 5Ji,5Jii) in comparison to control tumors and cultured cells, although the effect was more pronounced in tumors than cultured cells. It is likely that HIF1-α-dependent pathways are not so active in cultured PC-3 cells with adequate supply of oxygen and nutrients leading to discrepancy in pharmacological effects of Etn observed under *in vitro* and *in vivo* settings. This may partly explain the inconsistency in our immunoblotting data from cell and tissue lysates. Our data underscore the likelihood that Etn employs different cell-cycle and apoptosis regulators to mediate *in vivo* and *in vitro* effects due to differential extent of HIF1α signaling under the two conditions. Further, as alluded to earlier, Etn possibly exploits an unknown aspect of the *in vivo* cancer environment which may drive disparate mechanisms in cultured cells versus physiological systems. Furthermore, we found that CK inhibition abrogated Etn-mediated decrease in cellular glucose and glutamine content (Figs. 5Ji,5Jii). Taken together, these data suggest that Etn altered intracellular glucose and glutamine levels in tumors and cultured prostate cancer cells.

Having identified the effects of Etn on intracellular glucose and glutamine that impact glycolysis and other metabolic pathways, we performed 2-D gel electrophoresis of tumor lysates from control and Etn-treated animals to identify and characterize differentially-expressed proteins using LC-MS/MS analysis. We found two enzymes of glycolysis (glyceraldehyde-3-phosphate dehydrogenase and phosphoglycerate kinase-1) and one enzyme of glutamine metabolism (delta-1-pyrroline-5-carboxylate synthase) downregulated upon Etn treatment, which could exacerbate the metabolic crisis in Etn-treated tumor cells (Supplementary Fig. 8, Supplementary Table 5).

Etn alters cellular lipids and impairs mitochondrial integrity *in vivo*

Since Etn is a precursor of lipid constituents of membrane-bound cellular structures, we next asked if Etn altered structural integrity of membrane-bound organelles or adversely affected membrane fission-fusion events. Transmission electron microscopy (TEM) micrographs of tumors showed structural differences in mitochondria from control and Etn-treated groups. Specifically, mitochondria were elongated along with degraded matrix in treated tumors (Fig. 6Aii) compared to controls (Fig. 6Ai). We observed more osmiophilic granules in treated versus control tumors (Fig. 6Aiv) (Fig. 6Aiii) indicating lipid accumulation in treated-tumor cells. These results suggest that Etn treatment leads to lipid accumulation in cells, causes alteration of mitochondrial structure and induces lipid-mediated activation of cell death pathways. As TEM micrographs of Etn-treated samples showed many lipid granules, we next examined which lipids are specifically upregulated upon Etn treatment by a lipidomic analyses of tumors from control and Etn-treated groups.

We quantified a total of 402 lipids from various lipid classes such as phosphatidylethanolamine (PE), phosphatidylcholine (PC), phosphatidylserine (PS), lysophospholipids, ceramides, and sphingomyelin (SM). Levels of 21 lipids, out of 402, were increased in tumors from Etn-treated group (Fig. 6B). While these lipids mostly belonged to PE class (Fig. 6Bi), other lipids from the PS (Fig. 6Bii), PC (Fig. 6Bii) and SM (Fig. 6Biv) lipid classes were also increased. In summary, we infer that altered lipid levels can perturb lipid homeostasis upon Etn treatment resulting in changes in membrane properties that could initiate a cascade of events detrimental to cell survival.

Discussion

We have reported the preclinical development of Etn, including *in vitro* and *in vivo* efficacy, mechanism of action, pharmacokinetic evaluation, and toxicity measurements of its oral formulation for prostate cancer management. Taken together, our results demonstrate that Etn possesses desirable molecular traits and anticancer attributes with favorable ADMET properties for its development as an orally-deliverable broad spectrum cancer therapeutic. Etn exploits intrinsic overexpression of CK in cancer cells to convert into cytotoxic PhosE. Further, Etn treatment through downregulation of HIF1-α precipitates a bioenergetics/metabolic crisis, which activates p53-mediated signaling cascade culminating into cell death (Fig. 6C).

Essentially, malignant transformation involves extensive rewiring of metabolic circuitries to fulfill metabolic needs of rampantly proliferating cancer cells. HIF1-α plays a significant role in metabolic adaptation (shifting toward anaerobic glycolysis) of cancer cells by regulating glucose metabolism (33). HIF1-α controls expression level of glycolysis and gluconeogenesis enzymes including glyceraldehyde 3-phosphate dehydrogenase and phosphoglycerate kinase-1, that were found to be downregulated upon Etn treatment (33, 40). In cancer cells, glycolysis also provides intermediates for the synthesis of cellular building blocks (41). Glycolytic intermediates are used for the synthesis of amino acids such as alanine, serine and glycine. Recent reports demonstrate that HIF1-α regulates metabolism of glutamine, a key nutrient that maintains redox homeostasis, contributes to energy production and lipid biosynthesis (42, 43). Etn-mediated HIF1-α downregulation results in

reduced intracellular levels of glucose and glutamine uncoupling several metabolic pathways and leading to metabolic stress in cells. Downregulation of glycolysis and glutamine metabolism enzymes further exacerbates metabolic stress, which triggers p53-mediated cell death.

However, the question remains how Etn treatment downregulates HIF1-α resulting in a metabolic catastrophe in cancer cells that destines them to death. Since Etn treatment increases both PhosE and other lipids from various lipid classes, it is difficult to pinpoint the actual mediator of deleterious metabolic imbalance in cells. This is further complicated by lack of knowledge of biological implications of higher intracellular levels of PhosE. Phospholipids are one of the most abundant macromolecules present in cells and maintenance of cellular lipid homeostasis is crucial for cell survival. Further, cell membranes exhibit a tightly regulated asymmetric distribution of various lipids that is necessary for their proper functioning in various cellular processes such as endocytosis, cell signaling, membrane protein activation, etc. (44). Although lipid-mediated regulation of HIF1-α represents an untapped research area, there exists one report which suggests that changes in membrane properties can modulate HIF1-α expression by affecting EGFR function (45). This raises the possibility that accumulation of lipids may hamper the function of membrane proteins that are positive regulators of HIF1-α expression. Due to limited knowledge of the biological ramifications of high intracellular PhosE levels, further detailed investigations are indeed warranted to systematically delineate the molecular mechanism of HIF1-α downregulation upon Etn treatment.

We believe our study uncovers the previously unrecognized molecular link between the Kennedy pathway of lipid biosynthesis and cellular respiration/metabolism in cancer cells. Based on our results, Etn represents an extremely promising candidate for the development of an orally-deliverable non-toxic formulation for prostate cancer treatment by targeting glucose metabolism, a driver of cancer progression. Indeed we are excited about the prospects of our study in the context of recent articles spotlighting the agony and demand of cancer patients to access a compound (essentially, a variant of PhosE) that has been deemed as miracle cure for cancer (7, 8).

Supplementary Material

Refer to Web version on PubMed Central for supplementary material.

Acknowledgments

The authors would like to thank Dr. Charlie Benson and Samantha Simon from GSU for help with acquisition of immunotoxicity data.

Financial support: This work was supported by institutional grants to the PI (Aneja).

Abbreviations

ALPs	alkylphospholipids
BPR	blood plasma ratio

CK	choline kinase
CKI	choline kinase inhibitor
Etn	monoethanolamine
OCR	oxygen consumption rate
PC	phosphatidylcholine
PE	phosphatidylethanolamine
PhosE	phosphoethanolamine
PS	phosphatidylserine
RBC	red blood cell
RT	retention time
SGF	simulated gastric fluid
SIF	simulated intestinal fluid
SM	sphingomyelin

References

1. Pawson T, Warner N. Oncogenic re-wiring of cellular signaling pathways. Oncogene. 2007; 26:1268–75. [PubMed: 17322911]
2. Phan LM, Yeung SC, Lee MH. Cancer metabolic reprogramming: importance, main features, and potentials for precise targeted anti-cancer therapies. Cancer Biol Med. 2014; 11:1–19. [PubMed: 24738035]
3. Santos CR, Schulze A. Lipid metabolism in cancer. FEBS J. 2012; 279:2610–23. [PubMed: 22621751]
4. Baenke F, Peck B, Miess H, Schulze A. Hooked on fat: the role of lipid synthesis in cancer metabolism and tumour development. Dis Model Mech. 2013; 6:1353–63. [PubMed: 24203995]
5. van Blitterswijk WJ, Verheij M. Anticancer alkylphospholipids: mechanisms of action, cellular sensitivity and resistance, and clinical prospects. Curr Pharm Des. 2008; 14:2061–74. [PubMed: 18691116]
6. Cerella C, Sobolewski C, Dicato M, Diederich M. Targeting COX-2 expression by natural compounds: a promising alternative strategy to synthetic COX-2 inhibitors for cancer chemoprevention and therapy. Biochem Pharmacol. 2010; 80:1801–15. [PubMed: 20615394]
7. Drugs on demand. Nature. 2015; 527:410.
8. Ledford H. Brazilian courts tussle over unproven cancer treatment. Nature. 2015; 527:420–1. [PubMed: 26607521]
9. Ferreira AKMR, Neto SC, Chierice OG, Maria DA. Synthetic phosphoethanolamine induces apoptosis through caspase-3 pathway by decreasing expression of Bax/Bad protein and changes cell cycle in melanoma. J Cancer Sci Ther. 2011; 3:053–9.
10. Arruda, MSPd, Correa, MA., Venturini, J., Félix, MC., Rosis, AMBD., Galhiane, MS. The Effect of Phosphoethanolamine Intake on Mortality and Macrophage Activity in Mice with Solid Ehrlich Tumors. Braz. Arch. Biol. Technol. 2011; 54:1203–9.
11. Ferreira AK, Meneguelo R, Marques FL, Radin A, Filho OM, Neto SC, et al. Synthetic phosphoethanolamine a precursor of membrane phospholipids reduce tumor growth in mice

bearing melanoma B16-F10 and in vitro induce apoptosis and arrest in G2/M phase. Biomed Pharmacother. 2012; 66:541–8. [PubMed: 22902646]

12. Ferreira AK, Meneguelo R, Pereira A, Filho OM, Chierice GO, Maria DA. Synthetic phosphoethanolamine induces cell cycle arrest and apoptosis in human breast cancer MCF-7 cells through the mitochondrial pathway. Biomed Pharmacother. 2013; 67:481–7. [PubMed: 23773853]
13. Ferreira AK, Freitas VM, Levy D, Ruiz JL, Bydlowski SP, Rici RE, et al. Anti-angiogenic and anti-metastatic activity of synthetic phosphoethanolamine. PLoS One. 2013; 8:e57937. [PubMed: 23516420]
14. Ferreira AK, Santana-Lemos BA, Rego EM, Filho OM, Chierice GO, Maria DA. Synthetic phosphoethanolamine has in vitro and in vivo anti-leukemia effects. Br J Cancer. 2013; 109:2819–28. [PubMed: 24201752]
15. Ferreira AKMR, Pereira A, Mendonça Filho O, Chierice GO, Maria DA. Anticancer effects of synthetic phosphoethanolamine on Ehrlich ascites tumor: an experimental study. Anticancer Res. 2012; 32:95–104. [PubMed: 22213293]
16. Gerrit van Meer DRV, Gerald W. Feigenson. Membrane lipids: where they are and how they behave. Nat Rev Mol Cell Biol. 2008; 9:112–24. [PubMed: 18216768]
17. Gibellini F, Smith TK. The Kennedy pathway--De novo synthesis of phosphatidylethanolamine and phosphatidylcholine. IUBMB Life. 2010; 62:414–28. [PubMed: 20503434]
18. Dhakshinamoorthy S, Dinh NT, Skolnick J, Styczynski MP. Metabolomics identifies the intersection of phosphoethanolamine with menaquinone-triggered apoptosis in an in vitro model of leukemia. Mol Biosyst. 2015; 11:2406–16. [PubMed: 26175011]
19. Sushma Reddy Gundala CY, Rao Mukkavilli, Rutugandha Paranjpe, Meera Brahmbhatt, Vaishali Pannu, Alice Cheng, Reid Michelle D, Aneja Ritu. Hydroxychavicol, a betel leaf component, inhibits prostate cancer through ROS-driven DNA damage and apoptosis. Toxicol Appl Pharmacol. 2015; 280:86–96.
20. Karna P, Zughaier S, Pannu V, Simmons R, Narayan S, Aneja R. Induction of reactive oxygen species-mediated autophagy by a novel microtubule-modulating agent. J Biol Chem. 2010; 285:18737–48. [PubMed: 20404319]
21. Wallace TA, Prueitt RL, Yi M, Howe TM, Gillespie JW, Yfantis HG, et al. Tumor immunobiological differences in prostate cancer between African-American and European-American men. Cancer Res. 2008; 68:927–36. [PubMed: 18245496]
22. Varambally S, Yu J, Laxman B, Rhodes DR, Mehra R, Tomlins SA, et al. Integrative genomic and proteomic analysis of prostate cancer reveals signatures of metastatic progression. Cancer Cell. 2005; 8:393–406. [PubMed: 16286247]
23. Vanaja DK, Cheville JC, Iturria SJ, Young CY. Transcriptional silencing of zinc finger protein 185 identified by expression profiling is associated with prostate cancer progression. Cancer Res. 2003; 63:3877–82. [PubMed: 12873976]
24. Liu P, Ramachandran S, Ali Seyed M, Scharer CD, Laycock N, Dalton WB, et al. Sex-determining region Y box 4 is a transforming oncogene in human prostate cancer cells. Cancer Res. 2006; 66:4011–9. [PubMed: 16618720]
25. Arredouani MS, Lu B, Bhasin M, Eljanne M, Yue W, Mosquera JM, et al. Identification of the transcription factor single-minded homologue 2 as a potential biomarker and immunotherapy target in prostate cancer. Clin Cancer Res. 2009; 15:5794–802. [PubMed: 19737960]
26. Grasso CS, Wu YM, Robinson DR, Cao X, Dhanasekaran SM, Khan AP, et al. The mutational landscape of lethal castration-resistant prostate cancer. Nature. 2012; 487:239–43. [PubMed: 22722839]
27. Lapointe J, Li C, Higgins JP, van de Rijn M, Bair E, Montgomery K, et al. Gene expression profiling identifies clinically relevant subtypes of prostate cancer. Proc Natl Acad Sci USA. 2004; 101:811–6. [PubMed: 14711987]
28. Martinez MN, Amidon GL. A mechanistic approach to understanding the factors affecting drug absorption: a review of fundamentals. J Clin Pharmacol. 2002; 42:620–43. [PubMed: 12043951]
29. Caterina Palleria ADP, Chiara Giofrè, Chiara Caglioti, Giacomo Leuzzi, Antonio Siniscalchi, Giovambattista De Sarro, Luca Gallelli. Pharmacokinetic drug-drug interaction and their implication in clinical management. J Res Med Chem. 2013; 18:601–10.

30. Ramírez de Molina AR-GA, Gutiérrez R, Martínez-Piñeiro L, Sánchez J, Bonilla F, Rosell R, Lacal J. Overexpression of choline kinase is a frequent feature in human tumor-derived cell lines and in lung, prostate, and colorectal human cancers. Biochem Biophys Res Commun. 2002; 296:580–3. [PubMed: 12176020]
31. Vermes IHC, Steffens-Nakken H, Reutelingsperger C. A novel assay for apoptosis. Flow cytometric detection of phosphatidylserine expression on early apoptotic cells using fluorescein labelled Annexin V. J Immunol Methods. 1995; 184:39–51. [PubMed: 7622868]
32. Guidance Document on Using In Vitro Data to Estimate In Vivo Starting Doses for Acute Toxicity. 2001
33. Vaupel P. The role of hypoxia-induced factors in tumor progression. Oncologist. 2004; 9:10–7.
34. Semenza GL. HIF-1 and tumor progression: pathophysiology and therapeutics. Trends Mol Med. 2002; 8:S62–7. [PubMed: 11927290]
35. Faubert B, Vincent EE, Griss T, Samborska B, Izreig S, Svensson RU, et al. Loss of the tumor suppressor LKB1 promotes metabolic reprogramming of cancer cells via HIF-1alpha. Proc Natl Acad Sci USA. 2014; 111:2554–9. [PubMed: 24550282]
36. Marin-Hernandez A, Gallardo-Perez JC, Ralph SJ, Rodriguez-Enriquez S, Moreno-Sanchez R. HIF-1alpha modulates energy metabolism in cancer cells by inducing over-expression of specific glycolytic isoforms. Mini Rev Med Chem. 2009; 9:1084–101. [PubMed: 19689405]
37. Munoz-Pinedo C, El Mjiyad N, Ricci JE. Cancer metabolism: current perspectives and future directions. Cell Death Dis. 2012; 3:e248. [PubMed: 22237205]
38. Gohil VM, Zhu L, Baker CD, Cracan V, Yaseen A, Jain M, et al. Meclizine inhibits mitochondrial respiration through direct targeting of cytosolic phosphoethanolamine metabolism. J Biol Chem. 2013; 288:35387–95. [PubMed: 24142790]
39. Modica-Napolitano JSRP. Ethanolamine and phosphoethanolamine inhibit mitochondrial function in vitro: implications for mitochondrial dysfunction hypothesis in depression and bipolar disorder. Biol Psychiatry. 2004; 55:273–7. [PubMed: 14744468]
40. Semenza GL. Hypoxia, clonal selection, and the role of HIF-1 in tumor progression. Crit Rev Biochem Mol Biol. 2000; 35:71–103. [PubMed: 10821478]
41. Dang CV. Links between metabolism and cancer. Genes Dev. 2012; 26:877–90. [PubMed: 22549953]
42. Semenza GL. HIF-1 mediates metabolic responses to intratumoral hypoxia and oncogenic mutations. J Clin Invest. 2013; 123:3664–71. [PubMed: 23999440]
43. Sun RC, Denko NC. Hypoxic regulation of glutamine metabolism through HIF1 and SIAH2 supports lipid synthesis that is necessary for tumor growth. Cell Metab. 2014; 19:285–92. [PubMed: 24506869]
44. Fadeel B, Xue D. The ins and outs of phospholipid asymmetry in the plasma membrane: roles in health and disease. Crit Rev Biochem Mol Biol. 2009; 44:264–77. [PubMed: 19780638]
45. Lee SH, Koo KH, Park JW, Kim HJ, Ye SK, Park JB, et al. HIF-1 is induced via EGFR activation and mediates resistance to anoikis-like cell death under lipid rafts/caveolae-disrupting stress. Carcinogenesis. 2009; 30:1997–2004. [PubMed: 19789263]

Statement of translational relevance

Severe toxicity of currently-available chemotherapeutic agents and their intravenous infusion necessitating hospital visits limit their usefulness in cancer management. In this work, we have identified Etn (a precursor of phosphatidylethanolamine lipids) as an orally-deliverable anticancer agent whose non-toxicity conforms to FDA-approved standards. We demonstrated that Etn exhibits excellent pharmacokinetic and toxicokinetic profiles and anticancer activity, attributes that are most sought-after in orally deliverable anticancer drugs. Mechanistically, Etn targets energy and metabolite source (glucose and glutamine) of cancer cells which are unconventional targets in cancer therapy. These exciting results set the stage to systematically develop Etn as an IND (investigational new drug) candidate for cancer therapy. We are hopeful that clinical translation of Etn would bring an “effective, safer and kinder” oral therapy to cancer patients, and eliminate inconveniences associated with intravenous infusion of chemotherapeutic drugs that necessitates multiple hospital visits and admission.

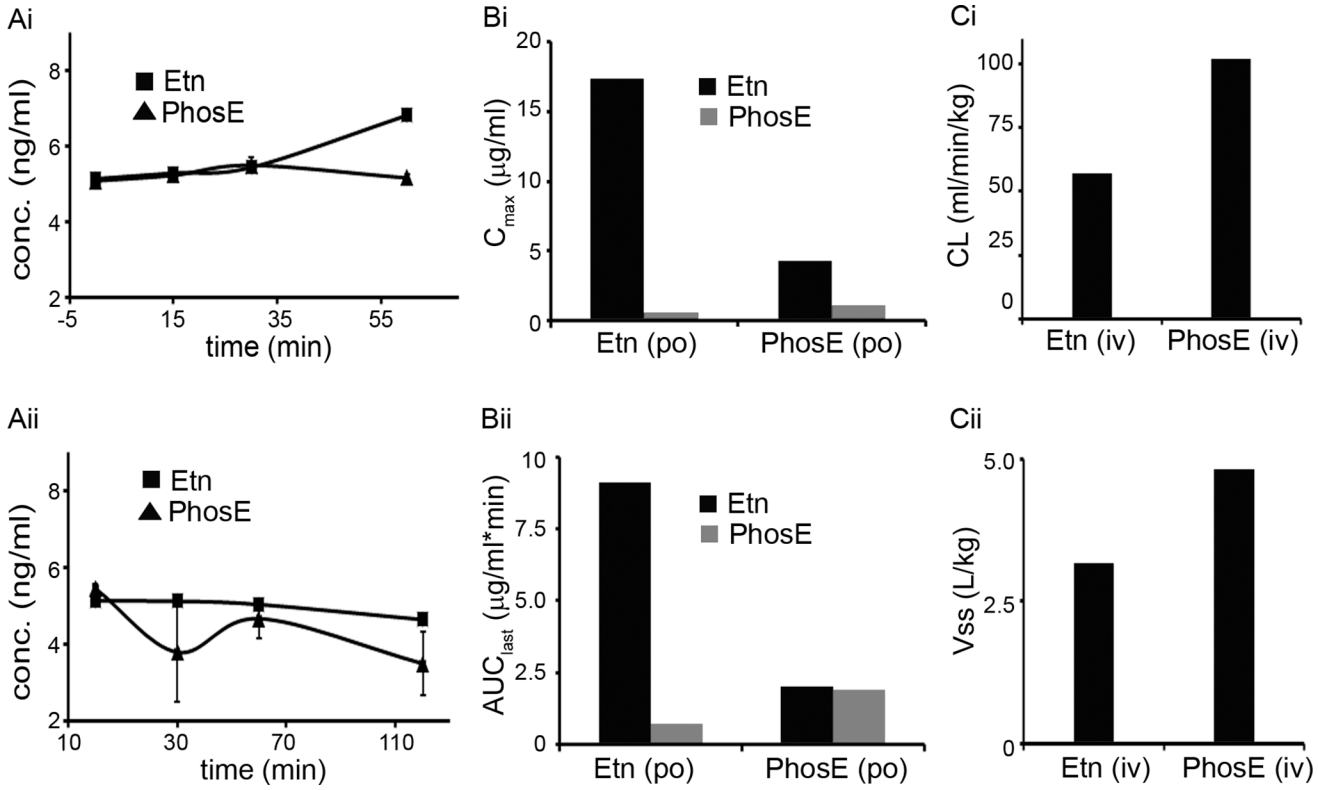

Figure 1.

Gastrointestinal stability and pharmacokinetic parameters of Etn and PhosE. Stability of Etn and PhosE in (Ai) SGF (pH 1.2) and (Aii) SIF (pH 6.8). Etn (10 µM) and PhosE (10 µM) were spiked into pre-incubated SGF and SIF. Samples (100 µl) were drawn at 0,15,30,60 min from SGF reaction-vials and at 0,30,60,120 min from SIF reaction-vials, quenched with acetonitrile, vortex-mixed, and centrifuged before supernatant analysis by LC-MS/MS analysis. (Bi) C_{max} and (Bii) AUC for Etn and PhosE upon oral administration of Etn and PhosE. (Ci) CL (clearance) and (Cii) Vss (volume distribution) for Etn and PhosE upon intravenous administration of Etn and PhosE. While PhosE and Etn were orally-fed at 60 and 40 mg/kg, respectively, intravenous administration were 3 and 2 mg/kg, respectively. For PK studies, a sparse sampling design with 3 mice per time point was used to collect blood samples at 5,10,15,30 min,1,2,3,4,5, and 6h in K_2EDTA-coated tubes. The pharmacokinetic parameters (AUC_{last}, C_{max}, CL and Vss) were calculated using non-compartmental analysis tool of Phoenix software (version 6.3).

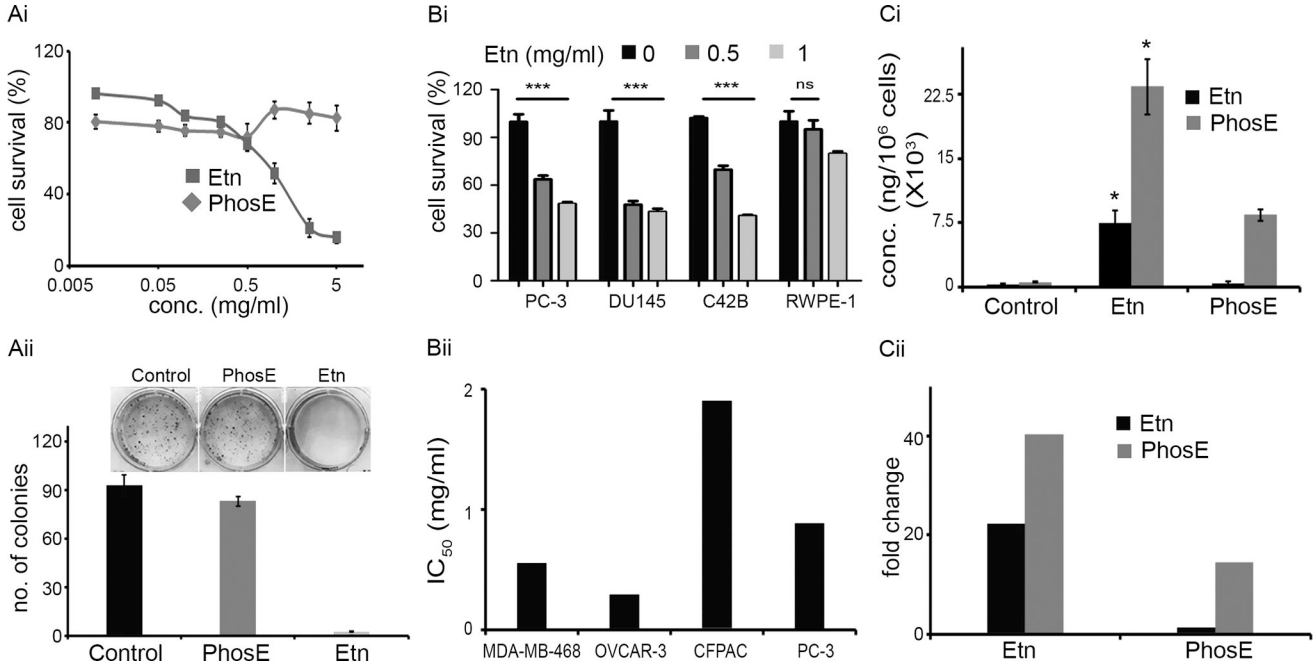

Figure 2.

Evaluation of *in vitro* anticancer efficacy and intracellular levels of PhosE and Etn. (Ai) Representative dose response curve for Etn and PhosE on the proliferation of PC-3 cells. The percentage of cell survival was measured by MTT assay after treating cells with increasing concentrations of Etn and PhosE for 48h at pH 7.4. (Aii) Bar graph representation and photograph of crystal violet-stained surviving colonies from the control, Etn and PhosE-treated groups. For clonogenic survival assay, PC-3 cells treated with 2 mg/ml Etn/PhosE at pH 7.4. (Bi) Antiproliferative effect of Etn treatment on prostate cancer cell lines (PC-3, DU145 and C42B) and normal cell line (RWPE-1). PC-3, DU145, C42B and RWPE-1 cells were treated with 0.5 and 1 mg/ml Etn for 48h at pH 7.4 followed by measurement of cell survival by MTT assay. (Bii) IC_{50} values of Etn treatment of cancer cell lines MDA-MB-486, OVCAR-3, CFPAC and PC-3. (Ci) Intracellular levels of Etn and PhosE upon treatment of PC-3 cells with 1 mg/ml Etn and PhosE. PC-3 cells were treated with PhosE or Etn at pH 7.4 for 48h and 1 million cells were collected for the quantification of PhosE and Etn by LC-MS/MS method. (Cii) Fold change in intracellular levels of Etn and PhosE in Etn and PhosE-treated cells in comparison to control cells. Values and error bars shown in the figure represent mean and SE respectively from three independent experiments (*, $p < 0.05$; ***, $p < .0001$ compared with respective controls).

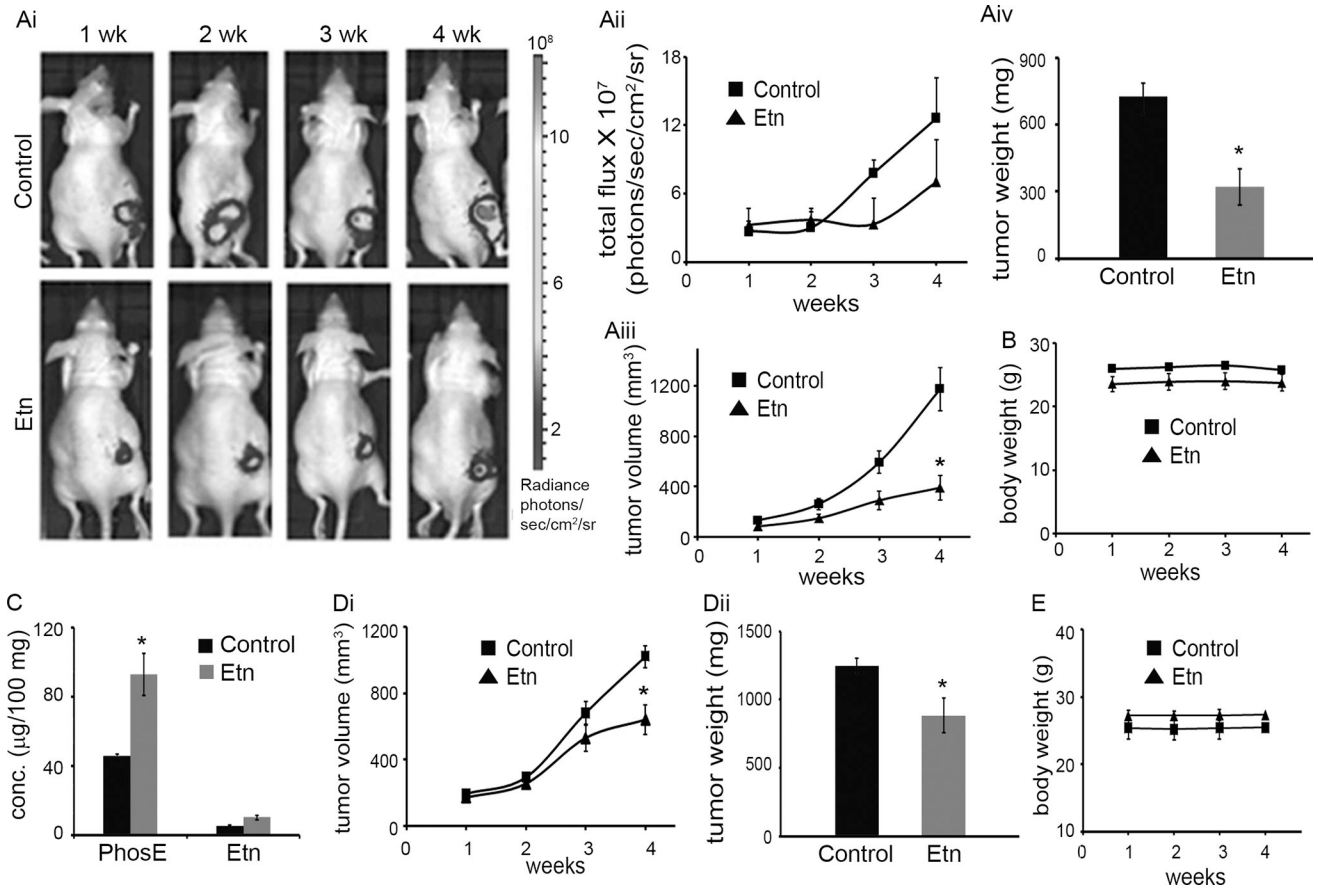

Figure 3.

Oral administration of 40 mg/kg Etn exhibited inhibition of human prostate tumor xenograft growth (PC-3-luc and DU145) in nude mice. PC-3-luc (1 million) or DU145 (2 million) cells in 100 µl PBS containing 25% Matrigel were subcutaneously injected in the right flank of 6–8 weeks old athymic male BALB/c mice to grow tumors. Mice with palpable tumors were randomly sorted in two groups of six mice each. Control group received vehicle (water) and treatment group received 40 mg/kg Etn adjusted to pH 5 with phosphoric acid by oral gavage for 4 weeks. (Ai) Representative bioluminescent images of one animal per group indicating progression of PC-3-luc tumor growth over 4 weeks in control and Etn-treated mice. (Aii) Graphical representation of the quantitative photon count from control and Etn-treated PC-3-luc tumor bearing mice for 4 weeks. (Aiii) PC-3-luc tumor growth monitored (by vernier calipers) over a period of 4 weeks. We observed ~67 % inhibition in tumor volume in comparison to control tumors upon oral administration of Etn for 4 weeks. (Aiv) Weight of PC-3-luc tumors from control and Etn-treated mice. Etn treatment resulted in ~55 % reduction in tumor weight in comparison to control tumors. (B) Body weight of vehicle and Etn fed PC-3-luc tumor bearing mice over a period of 4 weeks of treatment. (C) Intratumoral levels of PhosE and Etn in vehicle and Etn-fed PC-3-luc tumor bearing mice after 4 weeks. (Di) DU145 tumor growth monitored (by vernier calipers) over a period of 4 weeks. We observed ~42 % inhibition in tumor volume in comparison to control tumors upon oral administration of Etn for 4 weeks. (Dii) Weight of DU145 tumors from control and Etn-treated mice. Etn treatment resulted in ~29 % reduction in tumor weight in

comparison to control tumors. (E) Body weight of vehicle and Etn fed DU145 tumor bearing mice over a period of 4 weeks of treatment. Values and error bars shown in the figure represent mean and SE respectively (*, $p < 0.05$ compared with control).

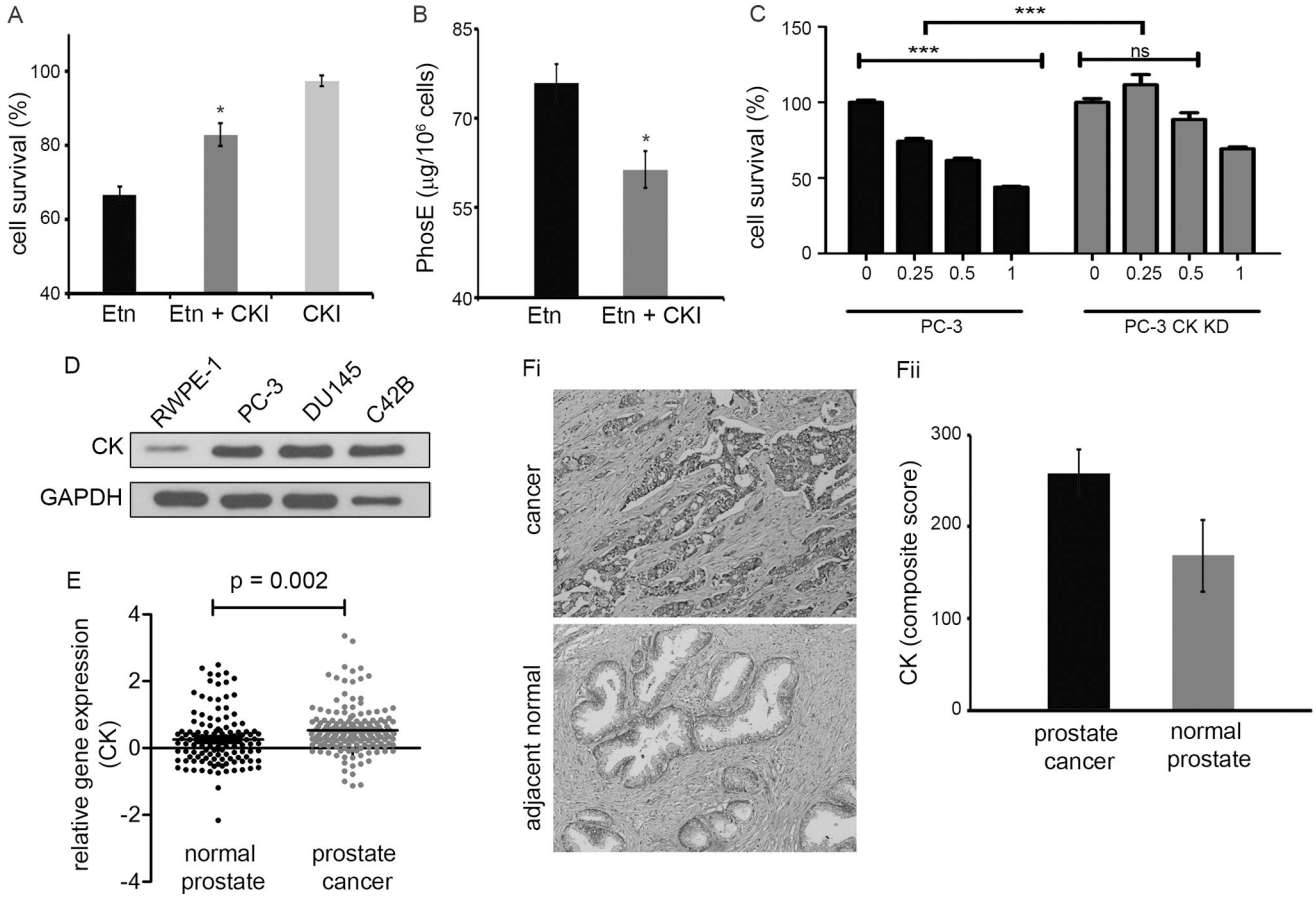

Figure 4.

Effect of choline kinase inhibition on Etn-induced inhibition of cell growth and intracellular levels of PhosE in PC-3 cells. (A) Proliferation of PC-3 cells upon Etn treatment in the presence and absence of choline kinase inhibitor (CKI). PC-3 cells were treated with 1 mg/ml Etn in the presence and absence of 1 μM CKI for 48h at pH 7.4 and cell survival was estimated by MTT assay. Choline kinase inhibition significantly abrogated Etn-induced cell death in PC-3 cells. (B) Intracellular levels of PhosE upon Etn treatment of PC-3 cells in the presence and absence of CKI. Choline kinase inhibition resulted in reduced conversion of Etn into PhosE in PC-3 cells. (C) Effect of Etn on cellular viability of PC-3 cells with CK knock down (KD) using siRNA approach. CK KD PC-3 cells were treated with 0.25, 0.5 and 1 mg/ml Etn for 48h at pH 7.4 followed by estimation of cell survival by MTT assay. (D) Choline kinase expression in prostate cancer cell lines (PC-3, DU145 and C42B) and normal prostate cell line (RWPE-1). GAPDH was used as a loading control. (E) Scatter-plot comparing choline kinase expression in normal and cancer tissue from prostate cancer patients ($p = 0.002$). The p value for statistical significance was set up as 0.05, while the fold change was defined as mean of all individual data points of analyzed datasets. (Fi) Micrographs showing immunohistochemical staining of choline kinase enzyme in normal and cancer tissue from prostate cancer patients. (Fii) Quantification (composite score) of choline kinase expression in normal and cancer tissue from prostate cancer patient. Five normal and five cancer tissue cases on TMA were scored for choline kinase staining

percentage and intensity and composite scores were calculated using two parameters. As shown in these figures, choline kinase enzyme is highly expressed in cancer tissue as opposed to normal tissue. Values and error bars shown in the figure represent mean and SE respectively from three independent experiments (*, $p < 0.05$ compared with Etn; ***, $p < 0.0001$ compared with control).

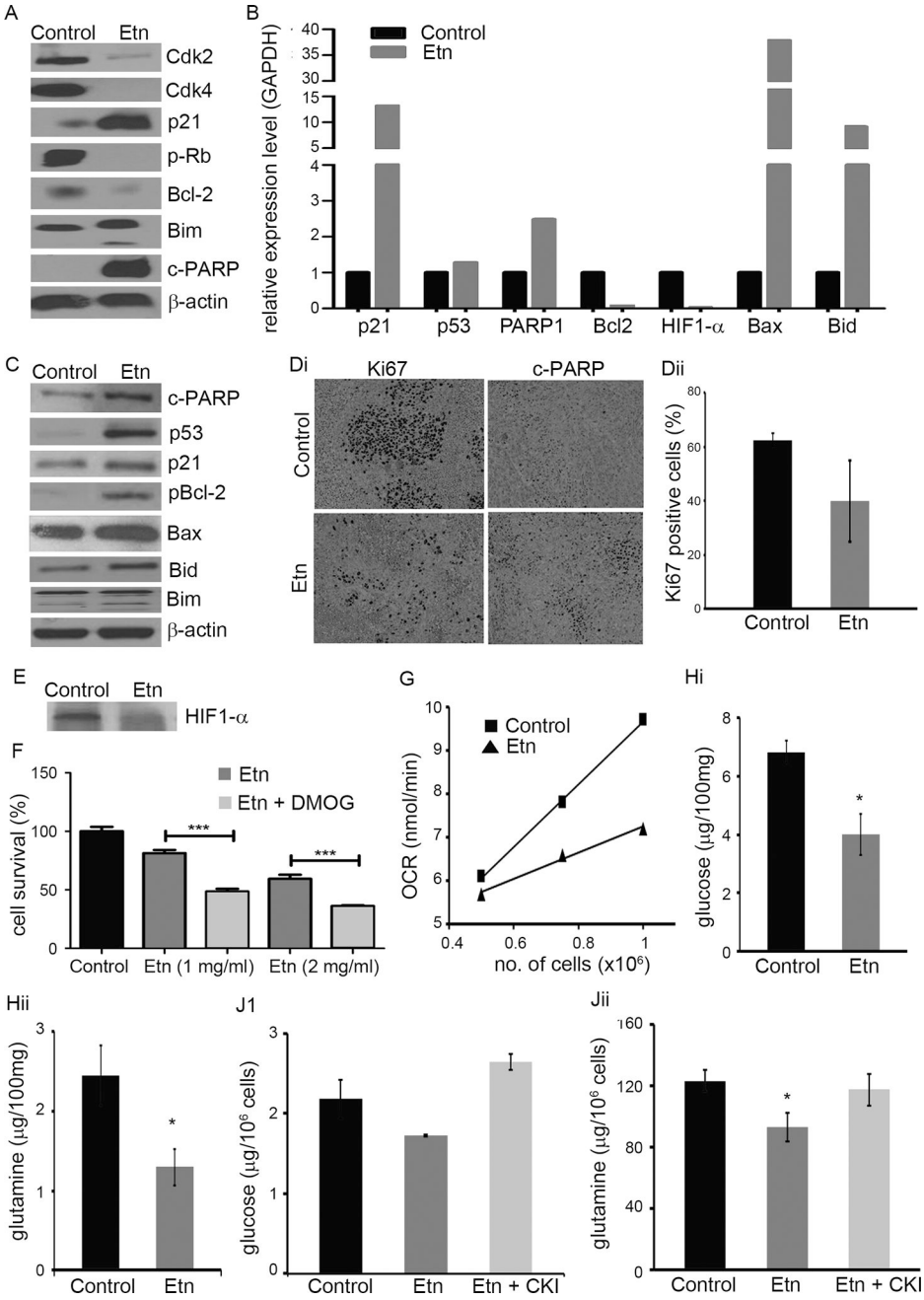

Figure 5.

Etn activates mitochondrially-mediated death pathways and affects oxygen consumption rate (OCR) and cellular metabolism in cancer cells. (A) Immunoblots of control and Etn-treated (2 mg/ml for 48h) PC-3 cell lysates for molecular regulators of cell-cycle (pRb, Cdk4, Cdk2, p21) and apoptosis (c-PARP, Bim, and Bcl-2). Beta actin was used as a loading control. (B) Relative transcripts of p21, p53, PARP1, Bcl-2, HIF1-α, Bax and Bid in control and Etn-treated (2 mg/ml for 48h) PC-3 cells. RNA samples were run on MOPS agarose gel to check integrity and two clear bands were observed for each sample. (C) Immunoblots of control and 40 mg/kg Etn-treated PC-3-luc tumors lysates for p53, p21, Bax, pBcl-2, c-PARP, Bim

and Bid. Beta actin was used as a loading control. (Di) Micrographs showing immunohistochemical staining of Ki67 and c-PARP in control and Etn-treated PC-3-luc prostate xenografts. (Dii) Quantification of Ki67 staining in control and Etn-treated prostate xenografts. (E) Effect of Etn treatment on HIF1-α expression level in PC-3 luc prostate xenografts. (F) Effect of HIF1-α stabilization on Etn-induced cell death in PC-3 cells. PC-3 cells were pre-treated with 35μg/mL DMOG (HIF1-α activator) for 4h followed by treatment with 1 and 2 mg/ml Etn and DMOG together for 48h and estimation of cell survival by MTT assay. (G) Effect of Etn treatment on oxygen consumption rate in PC-3 cells. PC-3 cells were treated with 2 mg/ml Etn for 48h at pH 7.4 and cells were suspended at a concentration of 0.5, 0.75 and 1 million/ml. OCR was measured by using oxygen electrode. Measurements were initiated by adding 500 μl of control and 2 mg/ml Etn-treated cell suspension at various concentrations into electrode chamber pre-equilibrated with 500 μl fresh media. The plot shows representative OCR as a function of cell number for control and Etn-treated cells. Intracellular glucose (Hi) and glutamine (Hii) levels in control and 40 mg/kg Etn-treated PC-3-luc tumors. Glucose and glutamine levels in control and Etn-treated tumors were estimated by LC-MS/MS method. (J) Effect of choline kinase inhibition on intracellular levels of glucose and glutamine in Etn-treated cells. Treatment of PC-3 cells with 2 mg/ml Etn for 48h reduced intracellular level of glucose (Ji) and glutamine (Jii) and this reduction in glucose and glutamine level was abrogated upon inhibition of choline kinase enzyme. Values and error bars shown in the figure represent mean and SE respectively from three independent experiments (*, $p < 0.05$ compared with control; ***, $p < 0.0001$ compared with Etn treatment).

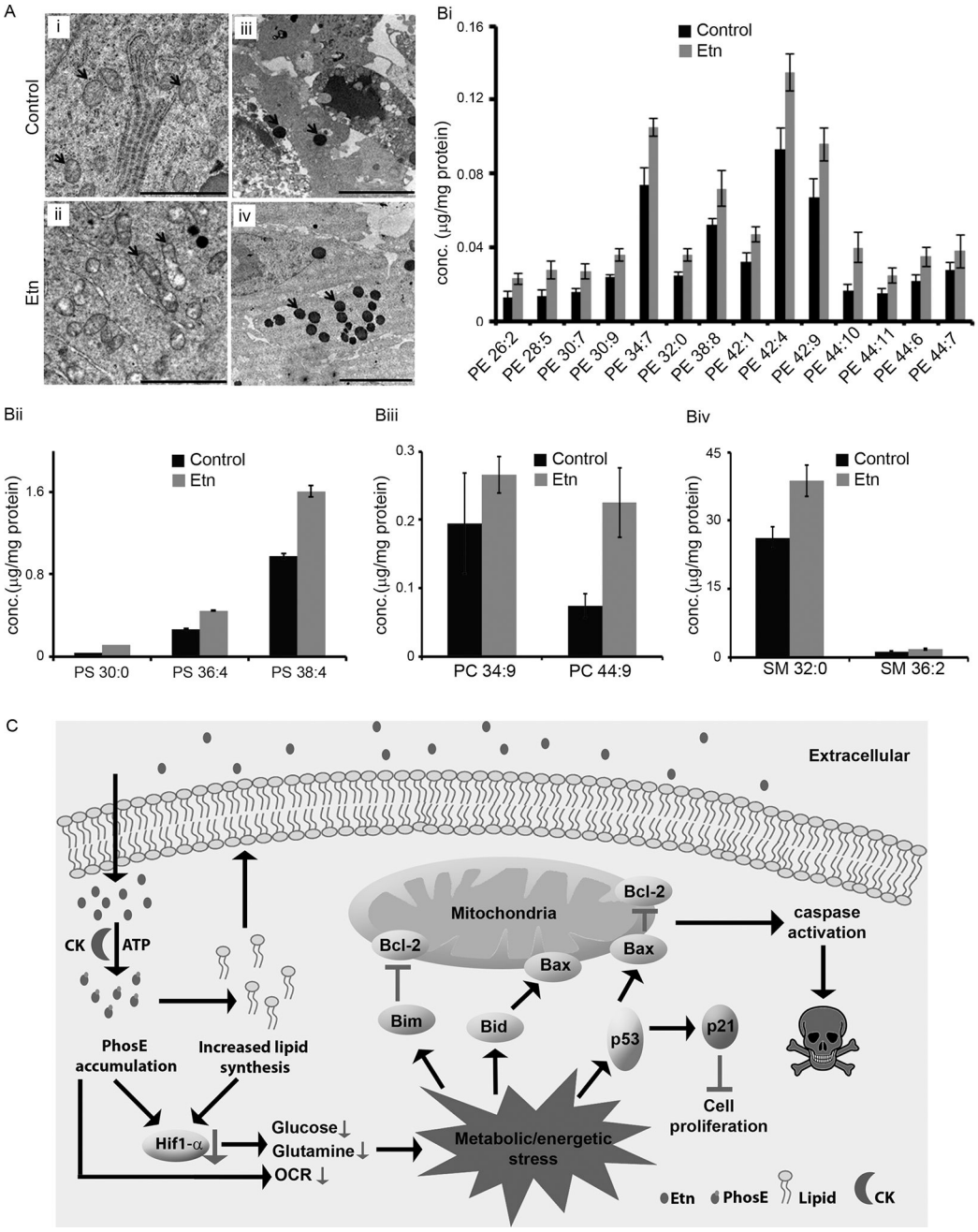

Figure 6.

Effect of Etn treatment on mitochondrial integrity and cellular lipids. (A) Representative transmission electron micrographs of control and 40 mg/kg Etn-treated tumors showing changes in mitochondrial morphology and accumulation of lipids upon Etn treatment. Ultrathin sections were cut on Boeckeler MTx ultramicrotome, counterstained with lead citrate, and examined on a LEO 906e transmission electron microscope. Mitochondria and accumulated lipid granules are highlighted by red arrows in the panel. Treated tumors showed elongated mitochondria with degrading mitochondrial matrix (Aii) and abundant lipid rich granules (Aiv) in comparison to control tumors (Ai, Aiii). Left panels, scale bar =

2 μM; Right panels, scale bar = 5 μM. (B) Etn treatment increases lipid levels in Etn-treated tumors. Levels of PE (Bi), PS (Bii), PC (Biii) and SM (Biv) lipids in control and Etn-treated tumors. In the abbreviation of lipid first and second numbers denote the number of carbon atoms and unsaturated bonds present in the lipid, respectively. Lipid amounts were quantified by LC-MS/MS analysis. Values and error bars shown in the figure represent mean and SE, respectively. (C) Schematic diagram depicting proposed model for anticancer activity of Etn in prostate cancer cells. We propose that accumulation of PhosE and phospholipid downregulates HIF1-α which precipitates a bioenergetics/metabolic crisis leading to activation of p53-mediated signaling cascade culminating into cell death.